

Spin entanglement in supramolecular structures

This article has been downloaded from IOPscience. Please scroll down to see the full text article.

2010 Nanotechnology 21 274009

(<http://iopscience.iop.org/0957-4484/21/27/274009>)

View [the table of contents for this issue](#), or go to the [journal homepage](#) for more

Download details:

IP Address: 155.185.12.220

The article was downloaded on 22/06/2010 at 13:45

Please note that [terms and conditions apply](#).

Spin entanglement in supramolecular structures

F Troiani¹, V Bellini¹, A Candini¹, G Lorusso^{1,2} and M Affronte^{1,2}

¹ CNR Institute of nanoSciences S3, Università di Modena e Reggio Emilia, via Campi 213/a, I-41125 Modena, Italy

² Dipartimento di Fisica, Università di Modena e Reggio Emilia, via Campi 213/a, I-41125 Modena, Italy

E-mail: marco.affronte@unimore.it

Received 9 January 2010, in final form 14 February 2010

Published 22 June 2010

Online at stacks.iop.org/Nano/21/274009

Abstract

Molecular spin clusters are mesoscopic systems whose structural and physical features can be tailored at the synthetic level. Besides, their quantum behavior is directly accessible in the laboratory and their magnetic properties can be rationalized in terms of microscopic spin models. Thus they represent an ideal playground within solid state systems to test concepts in quantum mechanics. One intriguing challenge is to control entanglement between molecular spins. Here we show how this goal can be pursued by discussing specific examples and referring to recent achievements.

(Some figures in this article are in colour only in the electronic version)

1. Introduction

Entanglement is a peculiarity of quantum systems and it represents one of the most fascinating aspects of quantum mechanics. It essentially consists in the impossibility of describing a quantum object without some knowledge of the rest of the system. More formally, it expresses the impossibility of factorizing the wavefunction of a composite system into the product of the wavefunctions of the components. For photons or cold atoms, as well as for a few solid state systems, entanglement is largely investigated, both theoretically and experimentally [1, 2]. These achievements underpin and stimulate exploitation of this property for new applications like quantum cryptography, teleportation and computation [50]. Besides, the controlled generation of entanglement between nanoscaled objects allows us to explore the boundary between quantum and classical behavior.

Molecular spin clusters represent a very interesting test bed in this context. In fact, they represent complex but finite systems whose structural and physical features can be tailored at the synthetic level and whose collective properties can be predicted by microscopic, albeit demanding, models. Recent achievements in supramolecular chemistry, experiments and modeling appear extremely encouraging in this field.

Here, we briefly review suitable molecules and linkers and illustrate methods used for the experimental determination

and rationalization of supramolecular systems. With the help of specific examples, we discuss different issues including the possibility of quantifying and probing entanglement in supramolecular systems; also, we provide hints for understanding and controlling the intermolecular coupling.

2. Molecular spin clusters

Molecular spin clusters are molecules consisting of a magnetic core and an external non-magnetic shell. Typically, the inner part is made of transition metal (hydro-) oxides bridged and chelated by organic ligands (typically chemical groups comprising light elements like carbon, oxygen, hydrogen, nitrogen, etc). Once synthesized, magnetic molecules are generally stable and they can be dissolved in solutions. From these, bulk crystals, comprising a macroscopic number of identical units aligned along specific crystallographic directions, can be obtained. In general, molecules do not interact with each other and the behavior of a bulk crystal turns out to be that of a collection of non-interacting, identical molecules. This allows us to use conventional solid state experimental techniques to investigate molecular features, which is certainly one of the keys for success of these molecular objects. In recent years, part of the interest in the field has been in developing protocols to graft and study arrays

of molecules on suitable substrates, aiming at addressing few or—eventually—single units.

Within each molecule, uncompensated electron spins are well localized on transition metals with quenched orbital moments (Fe, Mn, Cr, Ni, Cu, etc) and interact with each other by (super-)exchange coupling. This ferro or antiferromagnetic coupling dominates the intramolecular interactions and determines the pattern of magnetic eigenstates. Typically, the molecular spectra are well resolved at liquid-helium temperatures, while level crossings can be observed at magnetic fields of a few teslas, which are easily achieved in the laboratory. Anisotropy and antisymmetric terms in the spin Hamiltonian of the single molecule may arise from reduced local symmetries.

In the last few years, most of the interest has been devoted to molecules like the prototypical Mn_{12}ac or Fe_8 , with a high-spin ground state and high anisotropy barrier, that exhibit a characteristic hysteresis loop of the magnetization, justifying the name of single-molecule magnets (SMM) [5]. Intermolecular interactions can be reduced by diluting the molecules in solid crystals [6, 7] or in frozen liquid solution. Intermolecular dipolar interaction is limited in the case of antiferromagnetic molecular clusters, characterized by low-spin ground states. Among these, molecules with an $S = 1/2$ ground state, like V_{15} [8, 9] or the heterometallic Cr_7Ni rings [10, 11], represent prototypical examples of mesoscopic effective two-level systems.

A relevant aspect is the coherence of the molecular spin dynamics. Generally speaking, SMM represent an ideal playground to observe quantum phenomena at the mesoscopic scale [5]. The spectral definition of the SMM ground multiplet allowed us to perform electron spin resonance experiments in Fe_8 [12], Ni_4 [13] and Fe_4 [14]; these capabilities inspired schemes for performing quantum algorithms in Mn_{12}ac or Fe_8 [15], based on the massive exploitation of linear superpositions and quantum interference. A special case of coherent spin dynamics is that observed in single rare earth ions diluted in a crystalline matrix [16], which, however, do not represent a mesoscopic system. More recently, time-resolved experiments have shown that molecular electron spins can be coherently manipulated. In the case of antiferromagnetic clusters, Rabi oscillations on the 10^{-1} μs timescale have been observed in V_{15} while a decoherence time τ_d as long as 3 μs at 2 K has been directly measured in molecular Cr_7Ni rings [17]. Since the gate time τ_g to manipulate the effective $S = 1/2$ in real experimental conditions is of the order of 10 ns, it turns out that the figure of merit $Q = \tau_d/\tau_g$ exceeds 100 at 2 K for Cr_7Ni . For an isolated molecule the main source of decoherence remains the interaction with the nuclear spins both at the metal sites (specific isotopes) or in the organic environment (protons, fluoride, etc). Molecules typically comprise a few hundred atoms in well-defined positions, so the interactions between the electron and the nuclear spins can be rationalized for each molecule [18].

3. Chemical routes for linking molecules

Entangling spins in supramolecular structures, such as nanomagnet dimers or oligomers, requires at least two

separate steps: (1) the recognition of molecular building blocks with well-defined features and (2) the establishment of intermolecular magnetic coupling. Concerning the first step, the synthesis and the characterization of separate molecular units should be considered as a prerequisite. Ideally, each of the molecular units should be individually addressable; this implies that they should be either spatially or spectrally resolvable.

Different kinds of magnetic coupling between the units are compatible with the controlled generation of entangled states. Dipolar interaction is long range and might be desirable if one searches entanglement of a large collection of objects [19], but it is detrimental to control entanglement between a few molecular units within an oligomer, for it tends to couple molecules belonging to different oligomers. Therefore, local types of magnetic interaction, such as exchange, are preferable. In practice, when organic linkers are used to exchange-couple magnetic molecules there are two main risks: (1) to form polymeric networks that tend to undergo long range magnetic order and (2) magnetic states of a single moiety can be heavily perturbed by the chemical link. Recently different aromatic groups have been successfully used to selectively link molecular spin clusters. Timco and Winpenny in Manchester are currently using pyridine and pyrazole groups [3] while the group of Aromi is using β -diketonates ligands [20, 21].

Probably the first case of a molecular dimer reported in the literature is the $[\text{Mn}_4]_2$ [22, 23]. The individual moiety, $[\text{Mn}_4\text{O}_3\text{Cl}_4(\text{O}_2\text{CEt})_3(\text{py})_3]$ [24], comprises three Mn^{3+} and one Mn^{4+} coupled together to give a $S = 9/2$ ground molecular state and a uniaxial anisotropy. Two Mn_4 are linked through hydrogen bonds to form a Mn_4 dimer in which the magnetic states of each moiety are antiferromagnetically coupled to each other. The true problem of entanglement, however, was not considered there.

Another important case is that of heterometallic Cr_7Ni rings. Two species of Cr_7Ni rings have been synthesized: green [25] and purple [3] Cr_7Ni , after their respective color. The first attempt at linking two green Cr_7Ni rings was through the internal amine and different metal–organic groups [26]. From the chemical point of view this was successful since two rings have been selectively linked. Yet, the resulting magnetic coupling was vanishingly small except in the case where a Ru_2 dimer was introduced in the linker [27]. That was interesting since this Ru_2 dimer has redox properties and in principle its magnetic features can be switched by an external electrical stimulus; however, the effectiveness of such a scheme still needs to be proved. Important progress has been recently made by exploiting the fact that the chemical reactivity of the extra Ni is much faster than that of the rest of the Cr ions in the rings. Firstly, a chemical group was attached to the carboxylate at the Ni site in the green Cr_7Ni [4]; more recently, the nitrogen of the heterocyclic aromatic groups was directly linked to the Ni in the purple Cr_7Ni [3]. Starting from these, the choice of linker is virtually infinite [28]. In a first series of linked green Cr_7Ni rings, transition metal ions (M) or dimers were inserted in the linker, thus forming $\text{Cr}_7\text{Ni}-\text{M}_x-\text{Cr}_7\text{Ni}$ with $x = 1, 2$ [4]. By using purple Cr_7Ni , a family of $[\text{Cr}_7\text{Ni}]_2$ with short or longer linkers was obtained, thus allowing us to tune the strength of

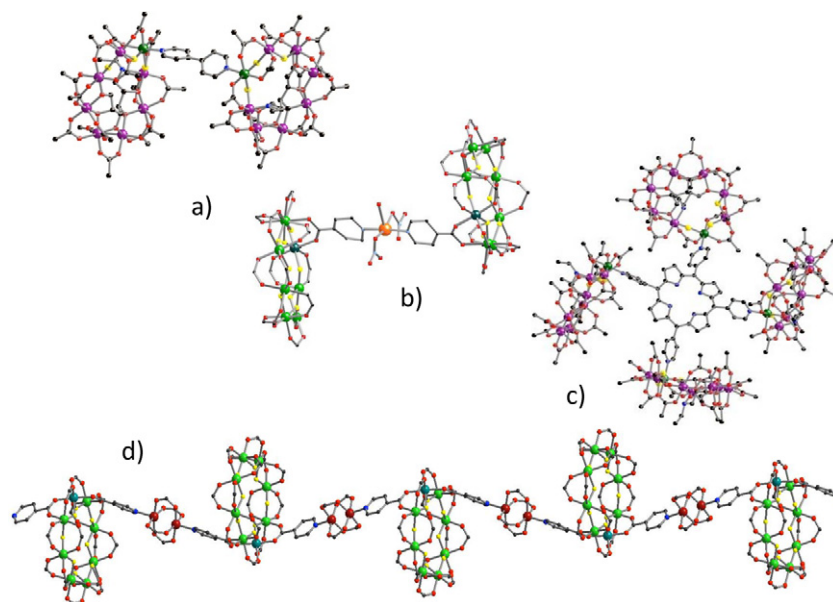


Figure 1. Supramolecular structures based on Cr_7Ni rings. (a) Two purple Cr_7Ni rings linked by bipyridine [3]; (b) two green Cr_7Ni rings linked by a metal–organic group containing a metal ion [4]; (c) a tetramer formed from purple Cr_7Ni rings [3]; (d) chain alternating Cr_7Ni rings with Cu ($s = 1/2$) ions.

the intramolecular coupling [3]. This strategy can also be used to synthesize molecular trimers, tetramers (with or without central metal ions) or chains alternating Cr_7Ni and metal ions or dimers (see figure 1) [3, 28].

4. Measuring and quantifying the magnetic coupling

The magnetic effectiveness of the intramolecular link can be experimentally evaluated. According to what was previously discussed, we first check the integrity of each molecular sub-unit and then we quantify the strength of the coupling. This may require the use of complementary experimental techniques and, possibly, the systematic comparison within a series of derivatives, from the individual molecule to complex aggregates. Magnetic susceptibility and magnetization loops are primarily used to clarify the nature of the ground state of the system while specific heat measurement directly evaluate the energy splitting of the lowest multiplets. Both need to be extended to very low temperatures (typically $T < 1$ K) where the magnetic coupling becomes observable. Electron paramagnetic resonance (EPR) spectra allow us to show transitions that are permitted only when the magnetic coupling is effective and they are sensitive to the anisotropy of the g factor.

As an example, figure 2 shows the magnetization loop $M(T, B)$ for a [purple- Cr_7Ni]₂ dimer with a bipyridylethylene ligand between two rings [29]. The $M(T, B)$ curves presented in the upper panels show the butterfly behavior, typical of the phonon-bottleneck regime, which becomes clearer as the sweeping rate dB/dt increases. Enlarging the magnetization curves $M(B)$ (lower panel), we can observe the presence of feeble knees, which are clearly evident by taking the derivative of magnetization dM/dB as shown in the insets. These

features are not present in the single purple Cr_7Ni ring and they are clearly due to the intramolecular coupling.

In figure 3 we consider another typical case, the Cr_7Ni –Cu– Cr_7Ni molecular trimer, for which the specific heat $C(T)$ provided direct evidence and quantification of the supramolecular coupling [4]. This system comprises two Cr_7Ni rings with an $S = 1/2$ ground state doublet and an $S = 3/2$ first excited multiplet, and one Cu ion with $S = 1/2$. The bumps in the $C(T)$ curve are the Schottky anomalies related to the energy splitting of specific multiplets. In 5 T the main anomaly is essentially related to the splitting between the $S = 1/2$ and $3/2$ multiplets, typical of the individual Cr_7Ni . The overlap between the specific heat of Cr_7Ni –Cu– Cr_7Ni (circles in figure 3) and that of two times the $C(T)$ of individual Cr_7Ni rings (dotted lines in figure 3) is direct evidence of the integrity of the molecular rings. In zero field, a Schottky anomaly clearly appears below 1 K for Cr_7Ni –Cu– Cr_7Ni but it is not present for individual rings for which the ground state is a Kramer doublet. This low temperature anomaly is a consequence of the coupling between the three effective spins $S = 1/2$ in Cr_7Ni –Cu– Cr_7Ni .

The sophisticated level of description of these mesoscopic systems provided by microscopic spin Hamiltonians merits a special mention. Briefly, the spin Hamiltonian of a single Cr_7Ni ring is [30]

$$\begin{aligned} \mathcal{H} = & J \sum_{i=1}^8 \mathbf{s}_i \cdot \mathbf{s}_{i+1} + \sum_{i=1}^8 d_i [s_{z,i}^2 - s_i(s_i + 1)/3] \\ & + \sum_{i < j=1}^8 D_{ij} [2s_{z,i}s_{z,j} - s_{x,i}s_{x,j} - s_{y,i}s_{y,j}] \\ & + \mu_B \sum_{i=1}^8 \mathbf{B} \cdot \mathbf{g}_i \cdot \mathbf{s}_i, \end{aligned} \quad (1)$$

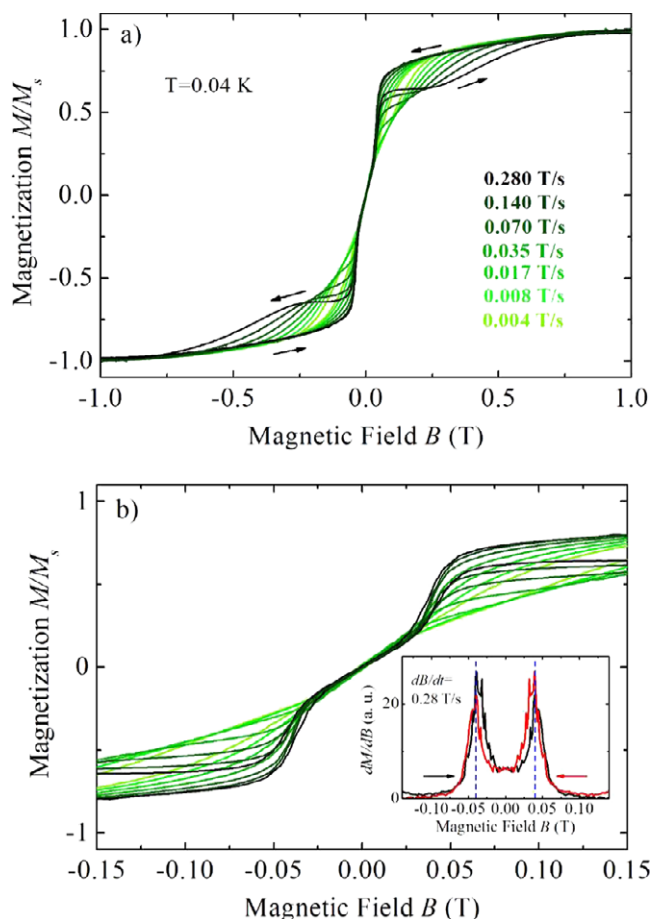


Figure 2. Experimental magnetization curves $M(T, B)$ taken for $[\text{Cr}_7\text{NiF}_3(\text{Etglu})(\text{O}_2\text{CtBu})_{15}]^{2-}$ (dipyet) (Etglu = *N*-ethyl-d-glucamine and dipyet = trans-1,2-dipyridylethene). (a) Data are taken at $T = 40$ mK and different sweeping rates of the magnetic field [29]. (b) Magnification of (a). (Inset) dM/dB versus B curve taken for $dB/dt = 0.28 \text{ T s}^{-1}$.

where the z axis coincides with the ring axis, site 8 corresponds to the Ni^{2+} ($s = 1$) ion, sites 1–7 are occupied by Cr^{3+} ($s = 3/2$) ions and $\mathbf{s}_9 \equiv \mathbf{s}_1$. The first term accounts for the isotropic exchange interaction, while the second and third ones are the dominant axial contributions to the crystal field and the intracluster dipole–dipole interactions, respectively. The last term represents the Zeeman coupling to an external magnetic field. The parameters entering the above Hamiltonian are determined by fitting the experiments performed with (ensembles of) single rings (see figure 3, for instance). Intra-ring interactions are also responsible for the anomalies above a few K in the supramolecular structures; the analysis of these features shows that the parameters are not affected by the intermolecular coupling introduced in the ring dimers and oligomers. Then, low temperature anomalies are described at a microscopic level by considering the interaction of the Cu spin center with Ni and Cr spins of each ring [4]. Considering also the projection of the rings' dipolar and crystal fields, the effective interaction can be written as

$$\mathcal{H} = J^* \mathbf{S}^{\text{Cr}_7\text{Ni}} \cdot \mathbf{S}^{\text{Cu}} + D_{\text{ex}}^* [2S_z^{\text{Cr}_7\text{Ni}} S_z^{\text{Cu}} - S_x^{\text{Cr}_7\text{Ni}} S_x^{\text{Cu}} - S_y^{\text{Cr}_7\text{Ni}} S_y^{\text{Cu}}] \quad (2)$$

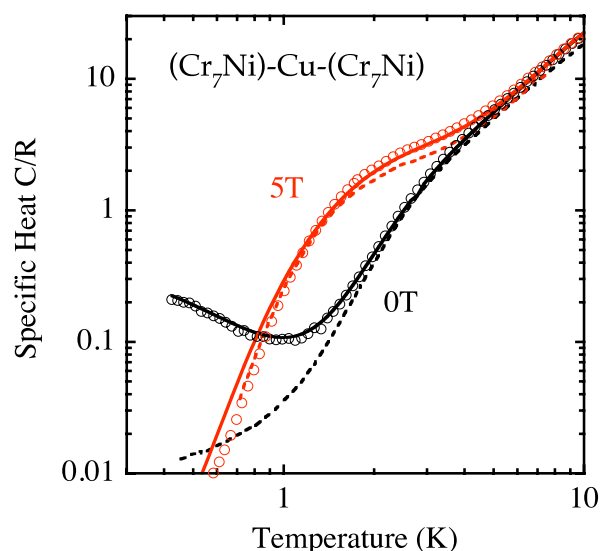


Figure 3. Low temperature specific heat of $\text{Cr}_7\text{Ni-Cu-Cr}_7\text{Ni}$ molecular trimer (circles). The—experimental—specific heat of two individual rings per unit cell is plotted as dotted lines. Continuous lines are calculated by spin Hamiltonian (see text) and they perfectly reproduce the experimental data.

for each $\text{Cr}_7\text{Ni-Cu}$ pair. The J^* and D_{ex} parameters are evaluated by simultaneously fitting complementary experimental results [4].

5. Understanding the magnetic coupling

How the organic linkers actually transmit spin information is an interesting issue that may help us to design organic linkers and new experiments. The series of $[\text{Cr}_7\text{Ni}]_2$ dimers discussed in a previous section is quite instructive from this point of view. The linker in those cases belongs to heteroaromatic organic groups (C-based benzene-like rings containing one or more nitrogens) that have been long studied and intensively used in the 1980s and 1990s in order to carry electronic and magnetic interactions between active molecular units through long (nm) distances, as compared to standard organic bridges such as single O or F atoms, hydroxides or carboxylates that, conversely, work on the atomic scale. Here the figure of merit, which discriminates between 'good' and 'bad' linkers, is the level of conjugation/delocalization of the electrons that carry the information. p electrons are distributed over two types of orbitals, the ones that bind the linker atoms together (sp^3 hybrids, with label σ) and π electrons that occupies resonant and delocalized bonds. Magnetic interaction is optimal when large overlap (both in space and in energy) between the spin-polarized orbitals of the magnetic centers and orbitals of the linker atom anchored to the magnetic centers is found; symmetry matching is also important. In principle, both σ and π electrons can carry magnetic interactions, although only with π electrons is delocalization strong enough to drive this interaction over long distances. Experimental observation of such interactions has been supported by numerical calculations, mostly performed by Hückel (extended) molecular orbital methods. Some

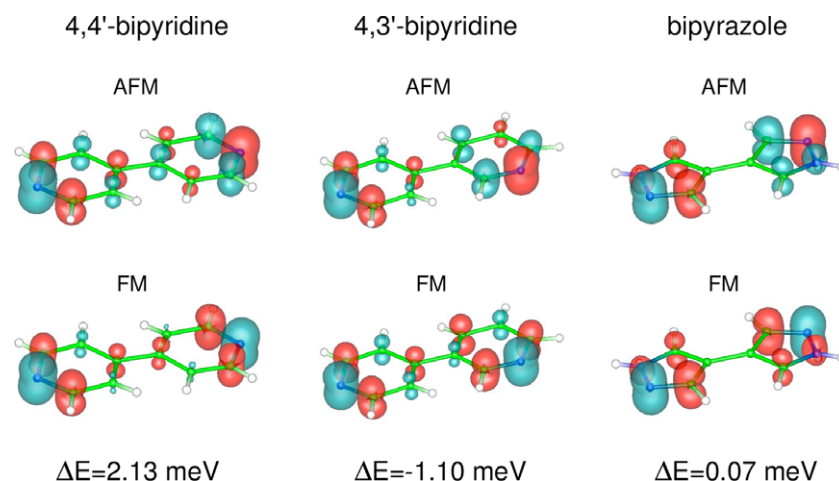


Figure 4. Spin density isosurfaces for isovalue of $+0.001$ electrons au^{-1} (blue color), and -0.001 electrons au^{-1} (red color), and FM–AFM energy splitting for 4,4'–bipyridine, 4,3'–bipyridine and bipyrazole bridges (see text for details).

general rules have been suggested in the literature: an interesting observation is that spin polarization of π electrons is found to proceed with an oscillating character, moving from one atom to the other through aromatic groups. This results in ferromagnetic or antiferromagnetic interactions between magnetic centers at the edges, depending on where they anchor [31, 32]. The strength of the interaction also obeys such an alternation rule, as discussed by Richardson and Taube [33], which has also been interpreted as arising from quantum interference over magnetic paths with different lengths [34]. As a matter of fact, alternation in spin and charge polarization through an aromatic linker can be theoretically explained by a superexchange mechanism discussed by McConnell [35] or, alternatively, by resonant theories, as found by Longuet-Higgins [36]. Another fact that has to be taken into account is that both occupied and unoccupied orbitals can play a role, as in charge transport [37]. Either π -occupied or unoccupied linker orbitals can be close in energy to the magnetic frontier orbitals, depending on whether the heteroaromatic linker is π -rich or π -poor; thus either HOMO- or LUMO-driven magnetic superexchange interactions can be promoted.

In order to illustrate this mechanism we present *ab initio* DFT calculations on model bicycle organic linkers, namely on bipyridine (both in the 4,4' and 4,3' configuration) and bipyrazole. Calculations have been performed with the NWChem quantum chemistry package [38]; an Ahlrichs valence double-zeta (VDZ) contracted Gaussian basis set has been used in conjunction with the hybrid B3LYP exchange and correlation functional. Let us focus on the 4,4' bipyridine bridge depicted in figure 4 and assume that the anchoring site is the N atom, more electronegative than C. Let us suppose also that the overlap between the magnetic frontier orbitals of the metal atoms anchored to the N sites with the N orbitals is such that a small spin polarization of $\pm 0.1 \mu_B$ is induced on the N atoms (the signs refer to a ferro- or antiferromagnetic coupling between these two moments). We impose such a spin moment by means of the constrained DFT method as discussed in [39]. We obtained spin-polarized states in N with both σ and π character, so that both symmetries can

contribute to the magnetic interaction, whereas most of the interaction is reasonably associated with the conjugated π -electron system. In figure 4 we plot the spin-polarized electron density isosurfaces for isovalues of ± 0.001 electrons au^{-1} in the case of antiferromagnetic and ferromagnetic coupling between the N spin moments. We can clearly see the alternation of spin polarization when moving from one atom to the next, following the bond paths. In order to demonstrate the rules discussed above, we also plot in figure 4 the spin densities for the 4,3' bipyridine and for bipyrazole organic bridges, always assuming that the metal is anchored to N sites, and that a spin moment of $\pm 0.1 \mu_B$ is transferred to N atoms. Changing from 4,4' bipyridine to 4,3' bipyridine, optimal coupling is attained when the spin polarization on the two N atoms has the same sign, i.e. magnetic centers are more favorable ferromagnetically coupled, as compared to the antiferromagnetic coupling attained for 4,4' bipyridine, as demonstrated by the larger spin polarization of the inner C atoms at the frontier between the two pyridines. In bipyrazole, the spin densities, for both the antiferro- and ferromagnetic states, do not reach the inner region and interference between the spin paths hinders magnetic interaction between the two sides of the bridge. In figure 4 we also report the total energy difference between the antiferromagnetic and ferromagnetic states, which indicates clearly how the size and the sign of the coupling are completely consistent with the reasoning above.

In order to predict the behavior of real dimeric complexes, the full systems, not just the bridge, have to be simulated. We analyze three supramolecular dimers of $[\text{Cr}_7\text{Ni}]_2$, which are characterized by identical magnetic molecular centers, two purple Cr_7Ni , but three different organic linkers, i.e. bipyridine, bipyrazole and bipyridylethylene [40]. Magnetic frontier orbitals are supplied by Ni ions and anchoring sites in the linkers are always N atoms. Ni(II) ions have nominally a $3d^8$ electronic configuration, so that only d orbitals with e_g symmetry are spin-polarized. Although in principle this should imply that only σ orbitals of the extended molecule are responsible for the spin interaction between the two rings, we observe that polarization of both σ and π orbitals in

the linker is present. σ polarization retains values only for the C atoms in the vicinity of the N atoms, while for more distant C atoms, only π orbitals attain a (small) spin polarization. Intramolecular Heisenberg J^* parameters, which quantify the interaction between the two Cr_7Ni molecules, can be estimated from several experimental methods (as described in section 4) or calculated by total energy (obtained by means of, for example, DFT-B3LYP calculations) difference methods. Here the microscopic interaction arises through the organic bridges between the two Ni spin moments, so that the relevant microscopic Hamiltonian is given by

$$H = J^* S_{\text{Ni}^1} \cdot S_{\text{Ni}^2}, \quad (3)$$

where the labels 1 and 2 indicate the Ni atoms belonging to different rings, and $S_{\text{Ni}^1} = S_{\text{Ni}^2} = 1$; J^* is then given by 1/2 of the total energy difference between the singlet and triplet states of the $(\text{Cr}_7\text{Ni})_2$ dimer, and positive values are relative to a preferred antiferromagnetic coupling between the rings, i.e. a singlet spin ground state. The calculated J^* values show a stronger magnetic coupling for bipyridine-bridged dimers ($J^* = 0.021$ meV) while for bipyrazole- ($J^* = 0.004$ meV) or bipyridylethylene- ($J^* = 0.002$ meV) bridged dimers interaction is sensibly smaller, in agreement with specific heat measurements that provide an estimate of the energy gap between the singlet and the barycenter of the triplet of 0.009 meV for bipyrazole-bridged and weaker ones (0.005 and 0.004 meV) for bipyrazole- and bipyridylethylene-bridged, respectively. In the case of bipyrazole, as anticipated above, quantum interference between the two paths seems to be responsible for the small J , despite the fact that the two Ni centers are closer to each other, as compared to bipyridine, because of the shorter length of bipyrazole. In the case of the bipyridylethylene bridge (not shown), the larger number of bonds that such an interaction should travel through plays a role, so that only a small fraction of spin polarization survives in the two facing C atoms in the center of the bridge [40]. These findings pave the way for a whole series of possible experimental investigations by systematically varying the organic bridges and the magnetic frontier atoms, in order to tune and choose the appropriate magnetic coupling for entanglement. The reasoning above, that has been derived in dimeric complexes, applies as well for trimeric or tetrameric systems, such as the ones described in previous section; in these cases, some additional difficulties might be represented by the many possible and simultaneous interaction paths, a circumstance that might prevent us prefiguring the magnetic properties of the systems by simple general conjectures, requiring that a full theoretical characterization has to be necessarily carried out.

6. Switchable molecular links

Although switchability is not mandatory for entanglement and spin manipulation can also be obtained between permanently coupled spins [41], we briefly discuss switchable organic linkers. We focus on three different switching mechanisms, namely a mechanical, an electric field-induced and a photochromic one. Critical issues like the switching rate or

preservation of coherence are far beyond the current discussion but, in the end, they will constitute possible bottlenecks for switchable linkers.

Transport through aromatic bicycles linkers have been demonstrated to depend on the structural conformation of the linker [42]. In the recent work of Quek *et al* [43], it has been demonstrated that transport properties of bipyridine-based molecular junctions are modified by elongating or compressing the junction; theoretical investigations have helped in attributing this finding to modification in the internal angles of the linkers, and in bond lengths and angles defining the pyridine–gold contact geometry. As discussed above, magnetic properties of supramolecular systems depend similarly on the structural conformation of the linker and of the linker–molecule contacts, leading to the idea of mechanical switching of the magnetic interactions. Another approach on the same line is the use of molecular shuttles [44] as possible switches.

Another possibility is to exploit a local electric field to rearrange the molecular orbitals and to suppress/enhance energy matching between orbitals of the linker and of the magnetic center. As discussed by Diefenbach and Kim [45] one can exploit the different spatial distributions of the molecular orbitals in the linker, and more precisely their different polarizabilities; upon the application of a (strong enough) electric field, the energetic order of the different orbitals might be modified, since a second-order Stark response might be very different for the different orbitals. In the case of low lying excited spin states, crossings between excited and ground states can be induced, which means that a different magnetic ground state can be fostered, that is, magnetic switching to on/off states can be achieved. Switchability of the linker is often used in other solid state systems like, for instance, quantum dots. In this respect, an interesting case was proposed considering a molecular poly-oxometallate $[\text{PMo}_{12}\text{O}_{40}(\text{VO})_2]^{9-}$ consisting of two $(\text{VO})^{2+}$ moieties with spin 1/2 separated by an Mo_{12} cage [46]. The cage may have different valence states and it can therefore be charged providing a switchable link between the two $S = 1/2$ spins. The implementation of a square-root-of-swap gate has been proposed [46] and experimental work is in progress in this direction.

The latter switching method is the one exploiting photoexcitation processes. Photochromic linkers belonging to the family of diarylethenes [47], undergoes reversible conformational changes upon irradiation in the visible or ultraviolet frequency range. They are optimal candidates because of their resistance, rapid photoresponse (in the range of picoseconds) and thermal stability of the two different isomers (up to 100 °C). Bonds form or break, and conjugation is suppressed or enhanced upon irradiation when moving from one isomer to the other; magnetic interaction path efficiency can, in this way, be controlled by photoirradiation. These molecular switches are excellent candidates for large-scale integration too, since photochromic complexes have been demonstrated to react both in solution and in two-dimensional lattices [48], and last but not least, to be compatible with coordination-driven self-assembly synthetic approaches.

7. Quantify and measuring entanglement in molecular spin clusters

The existence of a magnetic coupling between the molecular spin clusters does not guarantee *per se* that these are in an entangled state, but its form plays a crucial role in the controlled generation of entanglement. Therefore, the high degree of flexibility with which such coupling can be engineered through supramolecular chemistry represents a fundamental resource. To illustrate how the main concepts apply to the molecular systems, we consider two different approaches to the generation of entanglement in coupled Cr₇Ni rings, the first one based on equilibrium states ρ at low temperature, the second one on coherent manipulation of the system state by electron paramagnetic resonance (EPR) pulses. Since our interest is focused on entanglement between the total spins of the nanomagnets that compose the supramolecular structure, we shall refer to the total spins. In fact, if the intermolecular interaction is small compared to the intramolecular exchange coupling J , it can be treated at a perturbative level and mapped onto an effective Hamiltonian $\mathcal{H}_{\text{eff}}^{AB}$ that depends only on the total spins \mathbf{S}_α ($\alpha = A, B, \dots$) of the coupled molecules. Both the expression of $\mathcal{H}_{\text{eff}}^{AB}$ and the values of the effective parameters are deduced from the underlying microscopic model.

In order for the equilibrium density matrix to be entangled, one typically needs an intermolecular coupling Hamiltonian $\mathcal{H}_{\text{eff}}^{AB}$ with a non-factorizable ground state, and such that the energy separation from the first excited state is significantly larger than the lowest temperature at which relevant experiments can be performed. In the case of the (Cr₇Ni)₂ dimer ($S_A = S_B = 1/2$), the former condition can be achieved if the dominant term in the coupling Hamiltonian is an antiferromagnetic exchange interaction. Anisotropic intramolecular interactions give rise to additional effective terms, resulting in the following Hamiltonian: $\mathcal{H}_{\text{eff}}^{AB} = (J_{AB} - D_{AB})\mathbf{S}_A \cdot \mathbf{S}_B + 3D_{AB}S_z^A S_z^B$. For temperatures comparable with J_{AB} , the equilibrium state ρ includes contributions from all four lowest eigenstates $|S, M\rangle$ (S and M being the total spin and its projection along z , orthogonal to the plane of the molecules), with Boltzmann probabilities P_M^S . The entanglement between two $1/2$ spins can be quantified by the concurrence (\mathcal{C}), whose value ranges from 0 for a factorizable ρ to 1 for maximally entangled states [2]. In the present case, the expression of \mathcal{C} corresponding to the equilibrium state is

$$\mathcal{C}(P_M^S) = \begin{cases} \max\{|P_0^1 - P_0^0| - 2\sqrt{P_1^1 P_{-1}^1}, 0\} \\ \quad \text{for } \max\{P_0^1, P_0^0\} > \sqrt{P_{-1}^1 P_1^1} \\ 0 \quad \text{otherwise.} \end{cases} \quad (4)$$

In the presence of a magnetic field applied along the ring axis, the expression of the concurrence is

$$\mathcal{C}(\rho_{eq}^{AB}) = \frac{1 - e^{-\frac{J_{AB}}{k_B T}} \left(e^{\frac{D_{AB}}{k_B T}} + 2e^{-\frac{D_{AB}}{2k_B T}} \right)}{1 + e^{-\frac{J_{AB}}{k_B T}} \left[e^{\frac{D_{AB}}{k_B T}} + 2e^{-\frac{D_{AB}}{2k_B T}} \cosh\left(\frac{\bar{g}_{zz}\mu_B B}{k_B T}\right) \right]}, \quad (5)$$

where \bar{g}_{zz} is the z component of the effective g factor in the ground state $S = 1/2$ doublet of the Cr₇Ni ring (figure 5(a)).

According to this expression the molecular spin clusters A and B are entangled if the occupation of either $|0, 0\rangle$ or $|1, 0\rangle$ is sufficiently larger than all the others. In particular, in the limit $k_B T \ll (J_{AB} - D_{AB})$, the equilibrium state tends to the singlet ground state and $\mathcal{C} \simeq 1$. Therefore, the larger J_{AB} , the wider the temperature range in which thermal entanglement persists. In the present case, the range of desirable values of J_{AB} is, however, bounded from above by the characteristic energy of the intramolecular spin excitations. If this condition is not fulfilled, each nanomagnet within the dimer can no longer be regarded as effective two-level systems, for intramolecular excitations corresponding to higher spin multiplets enter the composition of the dimer's lowest eigenstates. The concurrence exponentially decreases with the magnetic field, which we assume for simplicity is oriented along z . In fact, the field energetically favors the factorizable ferromagnetic state ($M = 1$) and reduces the occupation of the singlet state. At zero temperature, an abrupt transition takes place as a function of B , at the level crossing between $|1, 1\rangle$ and $|0, 0\rangle$. As shown in figure 5(b), the effect of anisotropy on the concurrence is particularly evident in the vicinity of such crossing. In general, the concurrence cannot be easily expressed in terms of observable quantities. Its evaluation requires a knowledge of the system density matrix, which is either derived experimentally from quantum state tomography or indirectly through the determination and diagonalization of the system Hamiltonian. The latter approach is, in general, viable in the case of a few coupled molecular spin clusters, where a detailed knowledge of the system Hamiltonian can be achieved by simulating a number of experimental techniques, including specific heat, torque magnetometry, inelastic neutron scattering and electron paramagnetic resonance, as discussed in a previous paragraph.

The demonstration of quantum entanglement, however, can also be directly derived from experiments, without requiring knowledge of the system state. This can be done by using specific operators—the so-called *entanglement witnesses*—whose expectation value is always positive if the state ρ is factorizable. It is quite remarkable that some of these entanglement witnesses coincide with well-known magnetic observables, such as energy or magnetic susceptibility $\chi = dM/dB$. In particular, the magnetic susceptibility of N spins s , averaged over three orthogonal spatial directions, is always larger than a threshold value if their equilibrium state ρ is factorizable: $\sum_k \chi_k > Ns/k_B T$ [49]. This should not be surprising, since magnetic susceptibility is proportional to the variance of the magnetization, and thus it may actually quantify spin–spin correlation. The advantage in the use of this criterion consists in the fact that it does not require knowledge of the system Hamiltonian, provided that this commutes with the Zeeman terms corresponding to the three orthogonal orientations of the magnetic field $\beta = x, y, z$. As already mentioned, in the case of the (Cr₇Ni)₂ dimer, the effective Hamiltonian includes, besides the dominant Heisenberg interaction, smaller anisotropic terms, due to which the above commutation relations are not fulfilled. This might, in principle, result in small differences between the magnetic susceptibility and the entanglement witness $\bar{\chi}_{EW} \equiv$

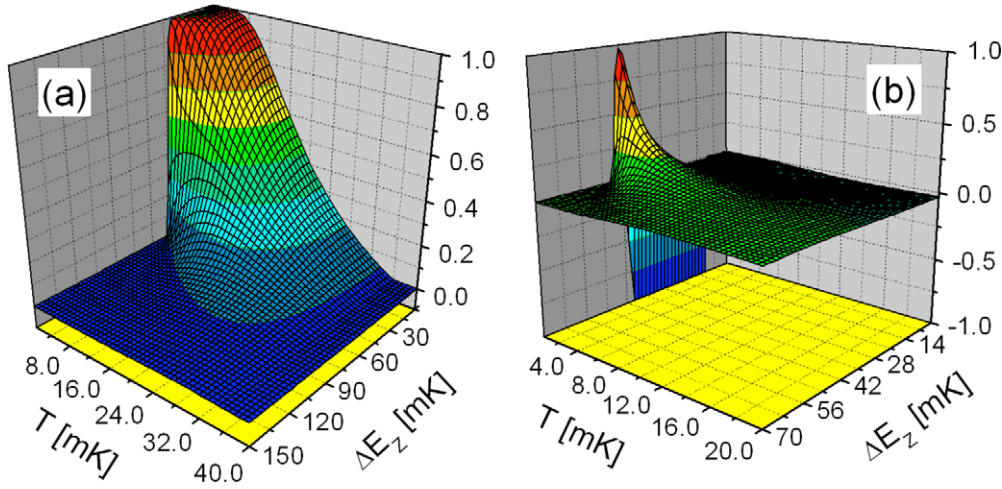


Figure 5. (a) Concurrence of the ring dimer as a function of temperature and of the Zeeman splitting induced by the applied magnetic field. The values of the physical parameters entering the effective Hamiltonian $\mathcal{H}_{\text{eff}}^{AB}$ are $J_{AB} = 40$ mK and $D_{AB} = 10$ mK. (b) Difference between concurrence in the presence of anisotropy and concurrence without anisotropy ($D_{AB} = 0$).

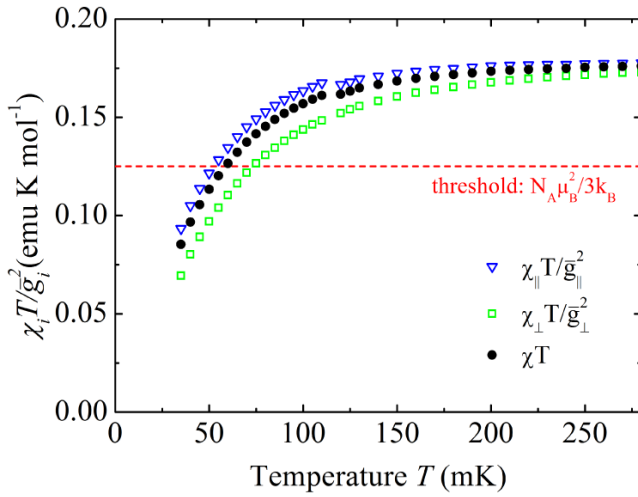


Figure 6. Magnetic susceptibility χ used as entanglement witness in the case of Cr_7Ni dimers. Temperature dependence of the measured χT product (triangles). χ_{\perp} (blue) is the component perpendicular to the largest surface of the crystal; this direction forms on average an angle of 16° with the z -axis, perpendicular to the ring plane. χ_{\parallel} (green) refers to the directions parallel to the crystal plane; rotation of magnetic field within this plane does not show changes in the magnetic response. The average $(\chi_{\perp} + 2\chi_{\parallel})/3$ (black dots) is compared with the threshold for a mole of dimers, $N_A \mu_B^2 / 3k_B$, in order to identify the temperature range ($T \leq 50$ mK) where the two rings are entangled [29].

$\sum_{\beta} [\sum_{\alpha, \beta} \langle S_z^{\alpha} S_z^{\beta} \rangle - \langle \sum_{\alpha} S_z^{\alpha} \rangle]$. Such a difference is, however, negligibly small if D_{AB} is small compared to J_{AB} and to the temperature (see figure 7). Magnetic susceptibility χ was used as an entanglement witness in the case of Cr_7Ni dimers [29]. In figure 6 the product χT is plotted versus temperature and compared with the expected threshold. In fact, in this system the ratio $J_{AB}/D_{AB} \simeq 4$ is large enough to make the difference between the magnetic susceptibility and the entanglement witness negligible.

An alternative approach to the generation of entangled states is represented by the application of suitable EPR pulse

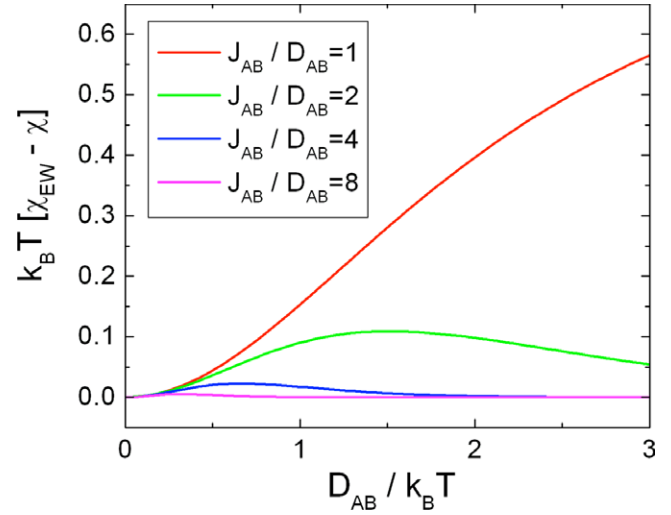


Figure 7. Difference between the entanglement witness χ_{EW} and the magnetic susceptibility for the ring dimer, derived from the effective Hamiltonian $\mathcal{H}_{\text{eff}}^{AB}$ in the limit $B \rightarrow 0$.

sequences to an initially unentangled state. Broadly speaking, this requires the implementation of a conditional dynamics, where the effect produced by a given pulse sequence of a (target) nanomagnet A depends non-trivially on the state of a (control) nanomagnet B . In the case where the dimer consists of two identical and equally oriented molecular spin clusters, limitations arise from the impossibility of individually addressing A and B . In fact, it is easy to verify that an effective Hamiltonian such as $\mathcal{H}_{\text{eff}} = \mathcal{H}_{\text{eff}}^{AB} + \sum_{\alpha=A,B} \mathbf{B}(t) \cdot \mathbf{g}_{\alpha} \cdot \mathbf{S}_{\alpha}$, with $\mathbf{g}_A = \mathbf{g}_B = \text{diag}(g_{\perp}, g_{\perp}, g_{\parallel})$, does not allow us to generate an entangled state such as $|S, 0\rangle$, starting from a factorized one such as $|1, \pm 1\rangle$. These limitations can be overcome in the case of an asymmetric system, where the coupling of the two effective spins A and B with the magnetic field are different, due either to the different chemical compositions of the two molecular spin clusters or to their different spatial orientations, combined with the anisotropy of the g tensor ($g_{\parallel} \neq g_{\perp}$).

Alternatively, the asymmetry of the intermolecular coupling can be exploited, such as that between the green and the purple derivatives of Cr₇Ni [28].

Analogous features allow the controlled generation of entangled states in tripartite systems. The (Cr₇Ni)–Cu–(Cr₇Ni) molecule, for example, behaves as a system of three effective 1/2 spins ($S_A = S_B = S_{Cu} = 1/2$) [4]. Entanglement between three parties can manifest itself in fundamentally different forms. In fact, two classes of equivalence have been defined, whose prototypical states are the so-called GHZ and W states, respectively. The GHZ states, whose expression in the $|M_A, M_B, M_C\rangle$ bases is: $|\Psi_{GHZ}\rangle = (|1/2, 1/2, 1/2\rangle + |-1/2, -1/2, -1/2\rangle)/\sqrt{2}$, maximize the genuinely tripartite entanglement, i.e. the one that cannot be reduced to pairwise correlations. The expression of the W states is instead: $|\Psi_W\rangle = (|1/2, 1/2, -1/2\rangle + |1/2, -1/2, 1/2\rangle + |-1/2, 1/2, 1/2\rangle)/\sqrt{3}$, and coincides with that of the $|S, M\rangle = |3/2, 1/2\rangle$. In order for the controlled generation of both $|\Psi_{GHZ}\rangle$ and $|\Psi_W\rangle$ to be possible, by applying suitable pulse sequences to an initial ferromagnetic state $|3/2, 3/2\rangle$, the degeneracy between the two transitions $|\Delta M| = 1$ within the $S = 3/2$ quadruplet needs to be broken. This is indeed the case for the (Cr₇Ni)–Cu–(Cr₇Ni) system, thanks to the anisotropic terms in the effective Hamiltonian (see equation (2)) and to the resulting zero-field splittings.

It is finally interesting to note that quantum correlations can also be present in the equilibrium state of the tripartite system described by the above effective Hamiltonian $\mathcal{H}_{\text{eff}}^{AC} + \mathcal{H}_{\text{eff}}^{BC}$, for suitable values of the parameters $J_{AC} = J_{BC}$ and $D_{AC} = D_{BC}$. If the inter-ring interaction is dominated by the exchange term ($J_{AC} \gg D_{AC}$), the anisotropy can be perturbatively included in first order, and the system eigenstates coincide with the vectors $|S_{AB}, S, M\rangle$ ($\mathbf{S}_{AB} = \mathbf{S}_A + \mathbf{S}_B$). In the case of a ferromagnetic coupling ($J_{AC} < 0$), the density matrix in the low temperature limit ($k_B T \ll |J_{AC}|$) is given by a statistical mixture of the $S = 3/2$ eigenstates. If $D_{AC} < 0$ [4], the three pairs of subsystems are all unentangled. In the case of an antiferromagnetic coupling between the rings, the ground state coincides with the state $|S_{AB} = 1, S = 1/2, M\rangle = (|1/2, -1/2, 1/2\rangle + |-1/2, 1/2, 1/2\rangle - 2|1/2, 1/2, -1/2\rangle)/\sqrt{6}$. If the tripartite system is cooled down to this state ($k_B T \ll J_{AC}, g\mu_B B$), each subsystem is entangled with the other two. In fact, the reduced density matrix of any two subsystems is real and takes the form

$$\rho_{\text{red}}^{\alpha\beta} = \begin{pmatrix} \rho_{11} & 0 & 0 & 0 \\ 0 & \rho_{22} & \rho_{23} & 0 \\ 0 & \rho_{23} & \rho_{33} & 0 \\ 0 & 0 & 0 & \rho_{44} \end{pmatrix},$$

where we refer to the basis $\{|1/2, 1/2\rangle, |1/2, -1/2\rangle, |-1/2, 1/2\rangle, |-1/2, -1/2\rangle\}$ and $\alpha, \beta = A, B, C$. For $\alpha\beta = AB$, the above matrix elements are: $\rho_{11} = 2/3$, $\rho_{22} = \rho_{33} = \rho_{23} = 1/6$ and $\rho_{44} = 0$. The resulting entanglement between the two rings is given by $\mathcal{C}(\rho_{\text{red}}^{AB}) = 1/6$. Each ring is also entangled with the Cu ion. In fact, for $\alpha\beta = AC$, the matrix elements are: $\rho_{11} = 1/6$, $\rho_{23} = -1/3$, $\rho_{22} = 2/3$, $\rho_{33} = 1/6$ and $\rho_{44} = 0$. This results in a finite concurrence, namely $\mathcal{C}(\rho_{\text{red}}^{AC}) = 2/3$.

8. Conclusions and perspectives

The list of cited references in this paper demonstrates that entanglement in supramolecular systems is an emerging topic of current interest and these earliest results show great potential. It is clear that advances in this field may arrive only from the combined effort of chemists, experimentalists and theoreticians.

From a synthetic point of view, the list of suitable molecular building blocks and of organic ligands working as efficient linkers is—if not infinite—certainly very long. We discussed the reasons why molecular Cr₇Ni rings, on the one hand, and heteroaromatic ligands on the other represent a very good starting point to build weakly interacting molecular complexes. The combination of the two (i.e. molecule + linker) is just limited by the rules of coordination chemistry, which may well bring about several interesting cases.

Experiments to characterize systems are certainly not routine but quite accessible. The range of molecular energies indeed spans between 0.01 and 10 K, which correspond to the energy of one electron in a magnetic field up to 10 T and frequencies ranging from 0.01 to 20 cm⁻¹, i.e. microwaves with low wavenumbers. Molecular spin clusters also represent an ideal test bed to perform experiments targeted at directly probing and quantifying entanglement in spin systems. Here we have just mentioned the use of magnetic susceptibility, independently measured along its three components, as an entanglement witness but other quantities, like specific heat or neutron scattering, may well do this job. In the future it will be certainly interesting to use pulsed electron spin resonance to address selectively molecular subensembles. Here the possibility of spectroscopically discerning different molecules will be certainly of interest. The design of specific pulse sequences will lead to implementation of quantum algorithms.

From the theoretical point of view, finite arrays of molecular spins are very appealing to develop models. Here one may wonder which conditions (forms of spin Hamiltonian, values of the spin $S \neq 1/2$, number of spin centers, etc) maximize/minimize entanglement. As mesoscopic systems, molecular spin clusters are paradigmatic cases to study the crossover between quantum and classical behavior.

Acknowledgments

We are indebted to Dr Grigore Timco and Professor Richard Winpenny (University of Manchester, UK) for sharing and discussing their results with us. Magnetization measurements were taken by microSQUID in collaboration with Dr Wolfgang Wernsdorfer in Grenoble (F). We thank Dr Alberto Ghirri and Christian Cervetti (CNR and University of Modena, I) for contributing to low temperature characterization and Dr S Carretta, Professors P Santini and G Amoretti (University of Parma, I) for stimulating discussions. This work is partially supported by the European project FP7-ICT FET Open ‘MolSpinQIP’ project, contract no. 211284.

References

- [1] Horodecki R, Horodecki P, Horodecki M and Horodecki K 2009 *Rev. Mod. Phys.* **81** 865
- [2] Amico L, Fazio R, Osterloh A and Vedral V 2008 *Rev. Mod. Phys.* **80** 517
- [3] Timco G A, McInnes E J L, Pritchard R J, Tuna F and Winpenny R E P 2008 *Angew. Chem. Int. Edn* **47** 9681
- [4] Timco G A et al 2009 *Nat. Nanotechnol.* **4** 173
- [5] Gatteschi D, Sessoli R and Villain J 2007 *Molecular Nanomagnets* (Oxford: Oxford University Press)
- [6] Abbati G et al 2001 *Chem.—Eur. J.* **7** 1796
- [7] Henderson J J, Ramsey C M, del Barco E, Stamatatos T C and Christou G 2008 *Phys. Rev. B* **78** 214413
- [8] Wernsdorfer W, Muller A, Maillly D and Barbara B 2004 *Europhys. Lett.* **66** 861
- [9] Bertaina S, Gambarelli S, Mitra T, Tsukerblat B, Muller A and Barbara B 2008 *Nature* **453** 203
- [10] Carretta S, Santini P, Amoretti G, Affronte M, Ghirri A, Sheikin I, Piligkos S, Timco G and Winpenny R E P 2005 *Phys. Rev. B* **72** 060403
- [11] Troiani F, Affronte M, Carretta S, Santini P and Amoretti G 2005 *Phys. Rev. Lett.* **94** 190501
- [12] Bal M, Friedman J R, Suzuki Y, Mertes K M, Rumberger E M, Hendrickson D N, Myasoedov Y, Shtrikman H, Avraham N and Zeldov E 2004 *Phys. Rev. B* **70** 100408(R)
- [13] del Barco E, Kent A D, Yang E C and Hendrickson D N 2004 *Phys. Rev. Lett.* **93** 157202
- [14] Schlegel C, van Slageren J, Manoli M, Brechin E K and Dressel M 2008 *Phys. Rev. Lett.* **101** 147203
- [15] Leuenberger M L and Loss D 2001 *Nature* **410** 789
- [16] Bertaina S, Gambarelli S, Tkachuk A, Kurkin I N, Malkin B, Stepanov A and Barbara B 2007 *Nat. Nanotechnol.* **2** 39
- [17] Ardavan A, Rival O, Morton J J, Blundell S J, Tyryshkin A M, Timco G A and Winpenny R E P 2007 *Phys. Rev. Lett.* **98** 057201
- [18] Troiani F, Bellini V and Affronte M 2008 *Phys. Rev. B* **77** 054428
- [19] Ghosh S, Rosenbaum T F, Aeppli G and Coppersmith S N 2003 *Nature* **425** 48
- [20] Sanudo E C, Cauchy T, Ruiz E, Laye R H, Roubeau O, Teat S J and Aromi G 2007 *Inorg. Chem.* **46** 9045
- [21] Barrios L A, Aguil D, Roubeau O, Gamez P, Ribas-Arino J, Teat S J and Aromi G 2009 *Chem.—Eur. J.* **15** 11235
- [22] Wernsdorfer W, Aliaga-Alcalde N, Hendrickson D N and Christou G 2002 *Nature* **416** 406
- [23] Hill S, Edwards R S, Aliaga-Alcalde N and Christou G 2003 *Science* **302** 1015
- [24] Hendrickson D N, Christou G, Schmitt E A, Libby E, Bashkin J S, Wang S, Tsai H L, Vincent J B and Boyd P D W 1992 *J. Am. Chem. Soc.* **114** 2455
- [25] Larsen F K et al 2003 *Angew. Chem. Int. Edn* **42** 101
- [26] Affronte M, Casson I, Evangelisti M, Candini A, Carretta S, Muryn C A, Teat S J, Timco G A, Wernsdorfer W and Winpenny R E P 2005 *Angew. Chem. Int. Edn* **44** 6496
- [27] Affronte M, Troiani F, Ghirri A, Carretta S, Santini P, Schuecker R, Timco G and Winpenny R E P 2007 *J. Magn. Mater.* **310** E501
- [28] Timco G and Winpenny R E P 2009 private communications
- [29] Candini A et al 2010 *Phys. Rev. Lett.* **104** 037203
- [30] Affronte M et al 2003 *Phys. Rev. B* **68** 104403
- [31] Cargill Thompson A M W, Gatteschi D, McCleverty J A, Navas J A, Rentschler E and Ward M D 1996 *Inorg. Chem.* **35** 2701
- [32] McCleverty J A and Ward M D 1998 *Acc. Chem. Res.* **31** 842
- [33] Richardson D E and Taube H 1983 *J. Am. Chem. Soc.* **105** 40
- [34] Marvaud V, Launay J-P and Joachim C 1993 *Chem. Phys.* **177** 23
- [35] McConnell H M 1963 *J. Chem. Phys.* **39** 1910
- [36] Longuet-Higgins H C 1950 *J. Chem. Phys.* **18** 265
- [37] Browne W R, Hage R and Vos J G 2006 *Coord. Chem. Rev.* **250** 1653
- [38] Bylaska E J et al 2007 *NWChem, A Computational Chemistry Package for Parallel Computers, Version 5.1* Pacific Northwest National Laboratory, Richland, WA 99352-0999, USA
- [39] Wu Q and van Voorhis T 2005 *Phys. Rev. A* **72** 024502
- [40] Bellini V and Affronte M, submitted
- [41] Troiani F, Ghirri A, Affronte M, Carretta S, Santini P, Amoretti G, Piligkos S, Timco G and Winpenny R E P 2005 *Phys. Rev. Lett.* **94** 207208
- [42] Venkataraman L, Klare J E, Nuckolls C, Hybertsen M S and Steigerwald M L 2006 *Nature* **442** 904
- [43] Quek S Y, Kamenetska M, Steigerwald M L, Choi H J, Louie S G, Hybertsen M S, Neaton J B and Venkataraman L 2009 *Nat. Nanotechnol.* **4** 230
- [44] Lee C-F, Leigh D A, Pritchard R G, Schultz D, Teat S J, Timco G A and Winpenny R E P 2009 *Nature* **458** 314
- [45] Diefenbach M and Kim K S 2007 *Angew. Chem. Int. Edn* **46** 7640
- [46] Lehmann J, Gaita-Arino A, Coronado E and Loss D 2007 *Nat. Nanotechnol.* **2** 312
- [47] Matsuda K and Irie M 2000 *J. Am. Chem. Soc.* **122** 7195
- [48] Jan van der Molen S, Liao J, Kudernac T, Agustsson J S, Bernard L, Calame M, van Wees B J, Feringa B L and Schenberger C 2009 *Nano Lett.* **9** 76
- [49] Wieśniak M, Vedral V and Brukner C 2005 *New J. Phys.* **7** 258
- [50] Nielsen M A and Chuang I L 2000 *Quantum Computation and Quantum Information* (Cambridge: Cambridge University Press)